A CFD Analysis to Investigate the Effect of Inserts on the Overall Heat Transfer Coefficient in a Concentric Tube Heat Exchanger

Naveedul Hasan Syed
Department of Chemical Engineering, University of Engineering & Technology, Peshawar, Pakistan
syednaveed@uetpeshawar.edu.pk (corresponding author)

Naseer Ahmed Khan
Department of Chemical Engineering University of Engineering & Technology, Peshawar, Pakistan
naseerahmedkhan@uetpeshawar.edu.pk

Naveed Ahmad
Department of Chemical and Materials Engineering, College of Engineering, Northern Border University, Arar, Saudi Arabia
naveed.ahmad@nbu.edu.sa

Murad Khan
Department of Chemical Engineering University of Engineering & Technology, Peshawar, Pakistan
muradkhan@uetpeshawar.edu.pk

Farooq Ahmad
Department of Chemical and Materials Engineering, College of Engineering, Northern Border University, Arar, Saudi Arabia
faroog.amin@nbu.edu.sa

Fiza Humayun
Department of Chemical Engineering, University of Engineering & Technology, Peshawar, Pakistan
fiza143humayun@gmail.com

Samiul Haq
Department of Chemical Engineering, University of Engineering & Technology, Peshawar, Pakistan
19pwche1381@uetpeshawar.edu.pk

Ibrahim Ali Alsayer
Department of Chemical and Materials Engineering, College of Engineering, Northern Border University, Arar, Saudi Arabia
I.Alsayer@nbu.edu.sa

Ibrahim Abdullah Altuwair
Department of Chemical and Materials Engineering, College of Engineering, Northern Border University, Arar, Saudi Arabia
Ibrahim.Altuwair@nbu.edu.sa

Received: 2 September 2024 | Revised: 18 September 2024 | Accepted: 22 September 2024

 DOI: https://doi.org/10.48084/etasr.8891

ABSTRACT

In the present study, a U-bend concentric tube heat exchanger has been modeled using Computational Fluid Dynamics (CFD) through ANSYS Fluent software to study the influence of different variables on the overall heat transfer coefficient (*U*). Following the successful validation of the CFD model, an analysis was conducted to examine the impact of five distinct star-shaped inserts on *U* enhancement in the U-bend concentric tube heat exchanger. The analysis demonstrated that the maximum *U* values, which were 381.21 W/m²K and 468.96 W/m²K, were attained at a hot water flow rate of 0.007 L/s when 14 mm plain and twisted star-shaped inserts were, respectively, employed. The incorporation of the inserts resulted in the generation of a secondary fluid motion within the tube, which in turn induced turbulence and consequently enhanced the heat transfer rate. However, the turbulence generated within the tube was attributed to the high pressure drop occurring there. The pressure drop within the inner tube was found to be 129.27 Pa and 149.44 Pa for the plain and twisted star-shaped inserts, respectively. The impact of elevated pressure drops for all five star-shaped insert types was examined and revealed to be the greatest for the 7 mm twisted insert, which was identified as the optimal choice for operational use. This conclusion was based on the observation that the twisted insert exhibited the highest *U* (390.89 W/m²K) at a pressure drop of 35.30 Pa, achieved at a hot water flow rate of 0.007 L/s.

Keywords-energy; finite element method; meshing; simulations; velocity vector

I. INTRODUCTION

The effective usage of available energy represents a crucial necessity in the contemporary era. In the context of heat energy, the devices in question are heat exchangers, which facilitate the transfer of energy from a hot fluid to a cold fluid through indirect contact [1-3]. Heat exchangers are further classified into the following categories: concentric tube, shell and tube, Plate Heat Exchanger (PHE), and spiral plate [4, 5]. Concentric tube heat exchangers represent one of the simplest types of heat exchangers, comprising two pipes arranged in a concentric configuration. These exchangers are compact in design and exhibit high heat transfer capabilities [6-8]. They are employed in a range of applications, that is, as preheaters, engine cooling circuits, condensers and heat recovery devices. Additionally, in the food and beverage industries, they are utilized for pasteurization and sterilization [9-11]. In order to reduce the size and cost of heat exchanger devices and conserve energy, numerous engineering techniques have been developed with the objective of enhancing *U* in heat exchangers. An increase in *U* results in the enhanced overall performance of a heat exchanger. In general, two broad categories of techniques may be employed to increase *U*: active and passive methods [12]. In active methods, *U* is improved by using some external power. In contrast, passive methods involve the incorporation of additional devices into the flow channels, such as different types and shapes of inserts, fins, and the utilization of rough surfaces [13].

In order to study the efficacy of passive techniques for enhancing the *U*-value of a given material, researchers have employed the use of a variety of shaped inserts. The latter have been tested in concentric tube heat exchangers, including twisted inserts, twisted tape inserts, plain inserts, tape inserts with holes, and tape inserts with baffles [14-17]. The incorporation of inserts results in turbulence within the tubes, which consequently increases *U*. However, twisted inserts generate relatively higher turbulence within the tube due to swirl flow conditions. The swirl motion generates a centrifugal force and produces a secondary flow inside the tube, which induces turbulence, and thus enhances *U*. In [14, 15], it has been demonstrated that the twisted tape inserts improve *U* by 8.9% in comparison to the plain inserts with holes and baffles. Similarly, conical twisted strip inserts have been employed to enhance *U*. The incorporation of inserts within the tubes has augmented the heat transfer rate. However, their usage also results in an elevated friction coefficient within the tube, which in turn gives rise to an increase in the pressure drop [16]. The inserts with holes and V-cuts have created a lower pressure drop than other inserts although this occurs at the cost of a relatively low heat transfer rate [15, 16]. Authors in [17] employed three twisted inserts with varying twist ratios and used convergent and divergent flow profiles to enhance the heat transfer rate. It was observed that *U* improved by up to 52% in comparison to a basic, unmodified heat exchanger. In a further experiment, authors in [18] passed hot air through the inner tube and cold water through the annulus of a concentric tube heat exchanger. The usage of helical inserts within the tube resulted in an observed increase in the heat transfer rate of up to 165% in comparison to the plain tube. Furthermore, a number of experimental studies have been performed on double tube heat exchangers using inserts of varying materials, including aluminum twisted tape. The studies demonstrated an increase in the heat transfer rate, although this was accompanied by an increase in the pressure drop [3, 11, 19]. Moreover, researchers employed modeling and simulation techniques to examine the impact of diverse process conditions and passive methods on the heat transfer rate and pressure drop within the tubes. The computational approaches employed by various researchers include CFD, convection-diffusion equations, and population balance methods [13, 20]. Computational studies facilitate the examination of internal system dynamics, with the principal objective of enhancing the efficiency of heat exchangers. CFD proved to be a highly valuable tool for the analysis and design of heat exchangers [3, 13], because it enables comprehensive simulations of fluid flow, heat transfer, and other significant phenomena within heat exchangers, offering insights that are either challenging or expensive to obtain through experimental methods [18, 20]. In CFD, the entire system or computational domain is divided into discrete elements or grids, and governing equations are applied to these elements to obtain numerical solutions regarding pressure distribution, temperature gradients, flow parameters

and flow patterns in a shorter time and at a lower cost [5, 21, 22].

Authors in [23] analyzed the heat transfer rate in a concentric tube heat exchanger using CFD while incorporating nanofluids within the tube and twisted tape turbulators within the annulus. An increase in the *U* of up to 6.03%, 16.74%, and 6.74%, was observed, with a 3% volume concentration of nanofluids, namely CNTS/H2O, Al2O3/H2O, and SiO2/H2O, respectively. Authors in [24] carried out a CFD analysis to investigate the influence of vortex generators on the enhancement of *U* in a concentric tube heat exchanger. The objective of the simulations was to study the spatial influence of the vortex generator and the effect of the Reynolds number in the annulus and inner tube of the heat exchanger. Evidence was provided for the increase in *U* resulting from the presence of a vortex generator within the tube and a high Reynolds number in the annulus. They also exhibited and explained the contours of high turbulence zones. Authors in [25] performed CFD simulations to investigate the effect of Reynolds numbers by changing the flow velocity at the inlets for both the hot and cold fluids, and concluded that CFD modeling has the potential to significantly enhance the design and efficiency of heat exchangers. In this research, a U-bend concentric tube heat exchanger was used to study *U* enhancement at different process conditions. This was done through both experimental and computational means. The unit was modeled using CFD through ANSYS Fluent software, and the simulation results were validated with the experimental results. The majority of studies have concentrated on the enhancement of *U* using inserts, with relatively little attention paid to the increase in pressure drop. It has been observed that there is an evident increase in pressure drop [11, 19]. However, there has been no suggestion of a suitable configuration of inserts for a specific type of heat exchanger. Moreover, this study marks the inaugural use of twisted star-shaped inserts of varying dimensions. Thus, an optimal size and configuration of the twisted star-shaped insert have been proposed, demonstrating enhanced *U* with a relatively minimal increase in pressure drop. Furthermore, CFD simulations have displayed that the secondary fluid velocity has been induced inside the inner tube as a result of the inserts.

II. EXPERIMENTAL SETUP AND METHODOLOGY

The experimental work was performed deploying a laboratory-scale U-bend concentric tube heat exchanger, serial number H900, manufactured by P.A. Hilton Ltd., as shown in Figure 1. The experimental unit consisted of an outer tube with a diameter of 22 mm and an inner tube with a diameter of 15 mm. The total length of the heat transmission zone was 1.50 m, with a heat transmission area of 0.067 m². Thermometers and temperature sensors were available for measuring the temperature of the water flowing in the inner tube and the annulus of the concentric tube heat exchanger. Additionally, a panel display was available for temperature measurement. Flow control valves were also provided for regulating the flow of water.

A. Operating Procedure

Prior to commencing the experiments, the experimental unit was subjected to a hydraulic test to ascertain the presence of any leaks. In the course of the experiments, distilled water was used, and the study was carried out at an ambient temperature of 25 °C and atmospheric pressure. The experiments were conducted utilizing a countercurrent flow arrangement, whereby hot water was circulated through the inner tube, while cold water was circulated through the annulus. The temperature at the inlet and outlet of the hot and cold water was measured using temperature sensors. The flow rates were adjusted employing the rotameters provided with the experimental unit. Table I portrays the range of the operational parameters over which the experiments were conducted.

Fig. 1. U-bend concentric tube heat exchanger H900.

TABLE I. OPERATING PARAMETERS

Operating parameters	Range
Cold water inlet temperature, Tc_{in} (°C)	298 – 305.50
Hot water inlet temperature, Th_{in} (°C)	315.50 – 356.50
Cold water flow rate, *Fc* (L/s)	0.0030 – 0.050
Hot water flow rate, *Fh* (L/s)	0.0070 – 0.073

B. CFD Modeling Approach and Governing Equations

CFD is a numerical method deployed to analyze the movement of fluids, mass transfer, heat transfer, and chemical reactions. The U-bend concentric tube heat exchanger was modeled using the governing equations, including mass conservation (i.e., continuity, momentum conservation, and energy conservation). The following assumptions were made during the modeling process: (a) the process is in a steady state, (b) the fluid is incompressible, (c) the fluid is stable within the computational domain, and (d) the inserts are fixed within the inner tube of the computational domain. The mass, momentum,

and energy conservation equations were solved following the finite volume method. The governing equations are:

$$\frac{\partial \rho}{\partial t} + \frac{\partial \rho u}{\partial x} + \frac{\partial \rho v}{\partial y} + \frac{\partial \rho w}{\partial z} = 0 \quad (1)$$

$$\nabla(\rho \overrightarrow{VV}) = -\frac{\partial p}{\partial x} + \frac{\partial \tau xx}{\partial x} + \frac{\partial \tau yx}{\partial y} + \frac{\partial \tau zx}{\partial z} + \rho g_x \quad (2)$$

$$\nabla(\rho \overrightarrow{VV}) = -\frac{\partial p}{\partial y} + \frac{\partial \tau yx}{\partial x} + \frac{\partial \tau yy}{\partial y} + \frac{\partial \tau yz}{\partial z} + \rho g_y \quad (3)$$

$$\nabla(\rho \overrightarrow{VV}) = -\frac{\partial p}{\partial z} + \frac{\partial \tau zx}{\partial x} + \frac{\partial \tau zy}{\partial y} + \frac{\partial \tau zz}{\partial z} + \rho g_z \quad (4)$$

where ρ is the density of fluid, *u, v, and w* the velocity components of fluid in the *x*, *y*, and *z* directions, respectively, τ is the viscous stress tensor, p the pressure of the working fluid, $\vec{V}$ the velocity vector, g the gravitational acceleration, and *T* the temperature of the fluid. Equations (1-4) are, equation of continuity, momentum – *x*, momentum – *y*, momentum – *z*, respectively.

Energy's' governing equation is:

$$\nabla.(\rho EV) = -p\nabla.\vec{V} + \nabla.(k\nabla T) + Q_h \quad (5)$$

where *E* is the total energy per unit mass, defined as:

$$E = h - \frac{p}{\rho} + \frac{v^2+u^2+w^2}{2} \quad (6)$$

where h is the specific enthalpy and Q_h is the volumetric heat source. Turbulent kinetic energy, k is:

$$\frac{\partial u_i k}{\partial x_i} = \frac{\partial}{\partial x_i}\left(\left(v + \frac{v_t}{\sigma_k}\right)\frac{\partial k}{\partial x_i}\right) + \Gamma - \varepsilon \quad (7)$$

where ν is the kinematic viscosity, v_t the turbulent viscosity, σ_k the turbulent Prandtl number for k, Γ the production of turbulent kinetic energy, and ε is the dissipation rate of turbulent kinetic energy.

The production of turbulent kinetic energy Γ is defined as:

$$\Gamma = -\bar{u}_i\bar{u}_j\frac{\partial u_i}{\partial x_j} = v_t\left(\frac{\partial u_i}{\partial x_j} + \frac{\partial u_j}{\partial u_i}\right)\frac{\partial u_i}{\partial u_i} \quad (8)$$

where $\bar{u}_i\bar{u}_j$ is the Reynolds stress tensor, and v_t the turbulent viscosity, defined as:

$$v_t = c_u\frac{k^2}{\varepsilon} \quad (9)$$

Turbulent Energy Dissipation, ε – epsilon, is:

$$\frac{\partial u_i \varepsilon}{\partial x_i} = \frac{\partial}{\partial x_i}\left(\left(v + \frac{v_t}{\sigma_k}\right)\frac{\partial \varepsilon}{\partial x_i}\right) - c_1\frac{\varepsilon^2}{k + \sqrt{v\,\varepsilon}} \quad (10)$$

where c_1 is the model constant, k is turbulent kinetic energy, and ε is the dissipation rate of turbulent kinetic energy.

C. Discretization of the System

Figure 2 depicts the computational domain of the concentric tube configuration, which is divided into two distinct mesh types, a coarse and a fine mesh. Figure 3 presents the discretized computational domain. The geometry was created using ANSYS Design Modeler 2022 R1. In order to create a mesh, the solver preferences were set to Fluent and a hex-mesh algorithm was applied. This resulted in the creation of a mesh comprising 2,617,198 elements, with an average element size of 10 mm. The insert edges were divided into four elements, while the pipe edges were divided into eighty elements, with an average size of one millimeter. A program-controlled orthogonal quality of a minimum of 2.5×10^{-2} was set to prevent divergence in elements. Additionally, inflation was configured to be program-controlled, and the target skewness was set to the default value of 0.9, whereas the smoothing was set to the high level.

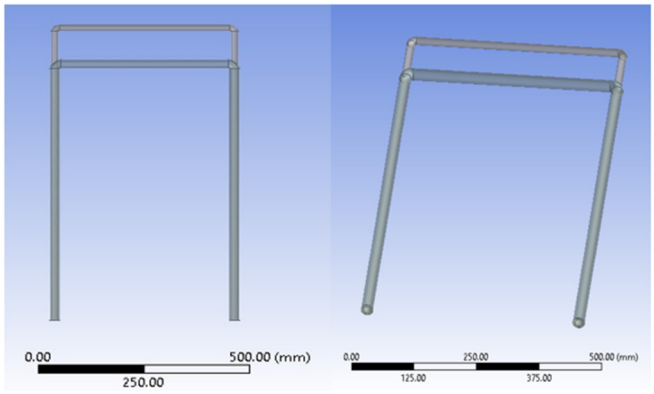

Fig. 2. Computational domain of U-bend concentric tube heat exchanger.

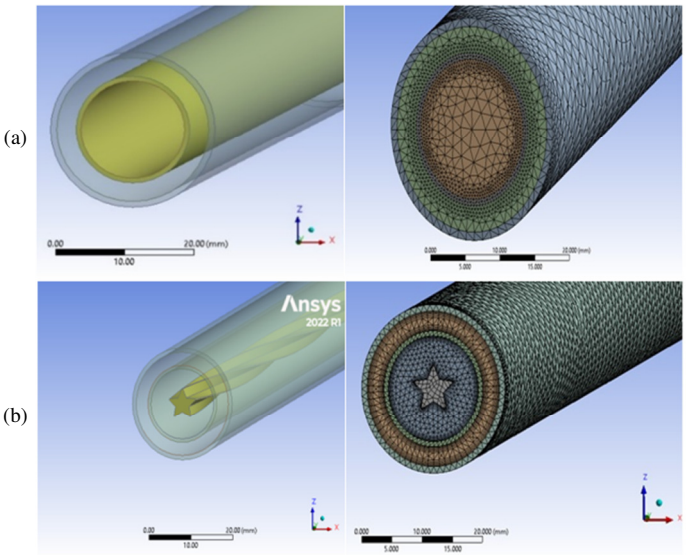

Fig. 3. Discretized computational domain: (a) inner and outer tubes (left), discretization of the inner and outer tubes (right), (b) inner and outer tubes with an insert (left), discretization of the inner and outer tubes with an insert (right).

The system was equipped with five distinct full-length star-shaped inserts, encompassing the entire computational domain. Two of the inserts were of a plain star shape, measuring 14 mm and 7 mm in diameter, while the remaining three were twisted star-shaped inserts, with a diameter of 14 mm, 7 mm, and 3.5 mm, respectively. Figure 4 illustrates the discretized plain star-shaped insert and the discretized twisted star-shaped insert.

D. Simulation Parameters

The simulation parameters can be seen on Table II.

TABLE II. SIMULATION PARAMETERS

Parameters/model	Numerical value/case setting
Turbulence model	Standard k-ε
Near-wall treatment	Standard Wall Function
Energy Equation	On
Scheme	Coupled
Spatial discretization gradient	Least squares cell based
Spatial discretization pressure	Second Order
Spatial discretization momentum	Second order upwind
Spatial discretization turbulent kinetic energy	Second order upwind
Spatial discretization dissipation rate	Second order upwind
Spatial discretization energy	Second order upwind
Inlet boundary condition	Mass Inlet (kg/sec)
Outlet boundary condition	Pressure outlet
Operating pressure	1.013×10^5 Pa
Wall boundary condition	No slip
Gravitational acceleration	9.81 m s^{-2}
Initialization	Standard
Convergence criteria	10^{-3} [–]
Maximum iterations	500 [–]

(a)

(b)

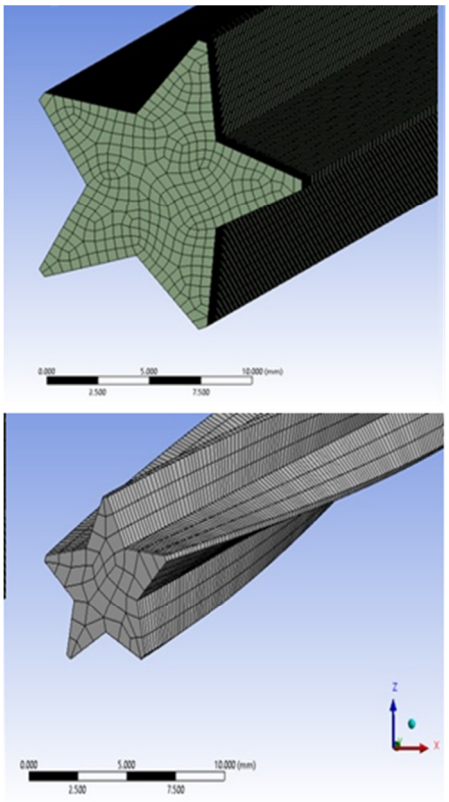

Fig. 4. Inserts: (a) discretized plain star shape, (b) discretized twisted star shape.

III. RESULTS AND DISSCUSSION

A total of 17 experiments were conducted on the experimental unit. Simulations were performed using the ANSYS Fluent software in accordance with the corresponding experimental conditions. In the course of the experiments, the temperatures of the cold and hot water at the outlets were determined. Similarly, the cold and hot water outlet temperatures were predicted in the simulations. The temperatures at the inlet and outlet were employed in the calculation of the Log Mean Temperature Difference (LMTD). Figure 5 shows a comparison of the LMTD between the experimental and simulation results. The simulation predictions exhibited a high degree of correlation with the experimental conditions, thereby demonstrating that the U-bend concentric tube heat exchanger was effectively modeled using CFD.

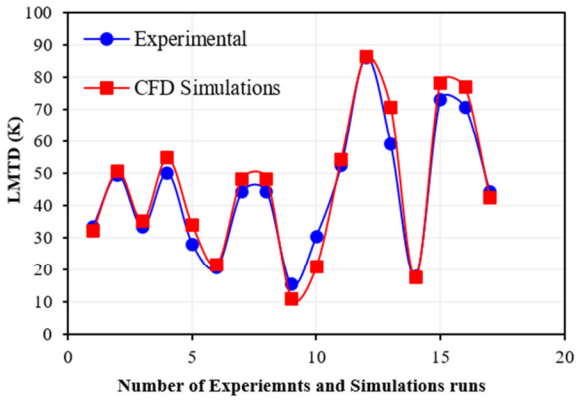

Fig. 5. Comparison of LMTD.

A. Effect of Hot Water Flow Rate on Overall Heat Transfer Coefficeint

Figure 6 shows a comparison between the experimental outcomes and the CFD simulations for the enhancement in U, with an increase in the hot water flow rate. The results presented concern three experimental runs in which the hot water flow rate was increased from 0.007 L/sec to 0.04 L/sec and to 0.073 L/sec, resulting in an increase in U by 265 W/m²K, 319.31 W/m²K, and 400.07 W/m²K, respectively. As the flow rate of the hot water increased, the turbulence within the inner tube also rose, leading to a heightened heat transfer rate. A comparable pattern of growth in U was discerned in the simulations, with U rising to 271.92 W/m²K, 314 W/m²K, and 411.46 W/m²K for the corresponding hot water flow rates. Figure 7 indicates that the experimental and simulation results were in good agreement.

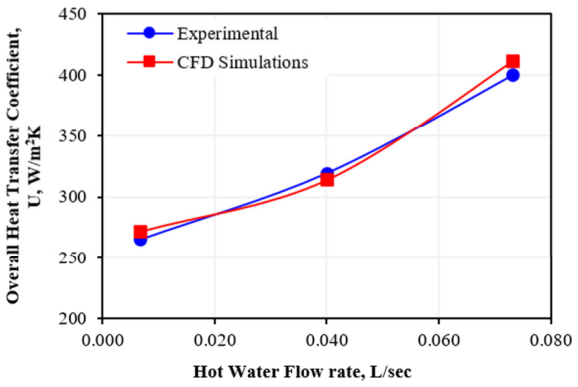

Fig. 6. U versus hot water flow rate.

B. Effect of Inserts on Overall Heat Transfer Coefficeint

Following the successful validation of the simulation results, five distinct types of star-shaped inserts were incorporated into the inner tube of the system to examine the impact of the inserts on *U* through the use of simulations. Table III delineates the process conditions for which simulations were conducted.

TABLE III. PROCESS CONDITIONS

Runs	Hot water flow rate (L/s)	Cold water flow rate (L/s)	Cold water temperature at inlet, Tc_{in} (K)	Hot water temperature at inlet, Th_{in} (K)
1	0.007	0.050	306.00	335.50
2	0.040	0.027	306.50	337.00
3	0.073	0.027	298.00	349.00

Figure 7 displays a comparison of the simulation results when the *U* was increased by including five different types of inserts in the inner tube of the U-bend concentric tube heat exchanger. The simulations used two plain star-shaped inserts with diameters of 7 mm and 14 mm and three twisted star-shaped inserts with diameters of 14 mm, 7 mm, and 3.5 mm. The first two runs show the validation of the results in which values of *U* equal to 312.34 W/m^{2}K, 319.31 W/m^{2}K, and 376.69 W/m^{2}K were obtained experimentally, as observed by the curve with filled circles, for runs 1, 2, and 3, respectively. Simulations without inserts were also carried out on the same process conditions, demonstrating an almost similar trend, with *U* values of 328.66 W/m^{2}K, 314.69 W/m^{2}K, and 369.65 W/m^{2}K, as seen by the curve with filled squares. The experimental and simulation results were in good agreement. In the third set of simulations, a 7 mm plain star-shaped insert was introduced into the inner tube. There was a slight increase in *U*, which was 337.96 W/m^{2}K, 323.50 W/m^{2}K, and 389.41 W/m^{2}K for the corresponding runs 1, 2, and 3, respectively. The increase in *U* was due to the turbulence caused by the insert inside the inner tube. However, the increase in *U* was not significant. In the fourth set of simulations, a 14 mm smooth start insert was introduced into the inner tube. The *U* increased significantly to 381.21 W/m^{2}K, 413.90 W/m^{2}K, and 571.33 W/m^{2}K for runs 1, 2, and 3, respectively. Subsequently, a 3.5 mm twisted start shape insert was introduced into the inner pipe of the U-bend concentric tube heat exchanger in the fifth set of simulations. The *U*-value increased to 362.68 W/m²K, 368.36 W/m²K, and 403.53 W/m²K for runs 1, 2, and 3, respectively. In this case, the *U*-value obtained from the triangular curve was higher than that obtained from the simulation in which a 7 mm plain star-shaped insert was used. However, it was less than that obtained from the simulation in which a 14 mm star-shaped insert was utilized. Similarly, in the sixth simulation run, a 7 mm twisted star-shaped insert was introduced into the system. The values of *U* obtained for the process conditions in runs 1, 2, and 3 were 390.89 W/m²K, 392.85 W/m²K, and 564.40 W/m²K, respectively. It can be observed that the *U* values obtained in this case, were very close to the values obtained in the case where a 14 mm plain star-shaped insert was used. Moreover, in the seventh set of simulations, a 14 mm twisted star shape insert was employed, resulting in a notable increase in *U* to values of 468.96 W/m²K, 533.56 W/m²K, and 571.33 W/m²K for the corresponding process conditions of runs 1, 2, and 3, respectively.

The simulation results demonstrate that the *U*-value increased when the inserts were instilled into the system. The inserts altered the direction of fluid flow within the tube, resulting in a secondary flow and subsequent turbulence, which led to an elevated heat transfer rate. However, with the twisted-shaped inserts, the heat transfer rate was higher, and *U* significantly increased. This was due to the fact that the twisted portion of the insert generated swirl motion, which induced relatively high turbulence and consequently resulted in a higher heat transfer rate and an overall elevated heat transfer coefficient.

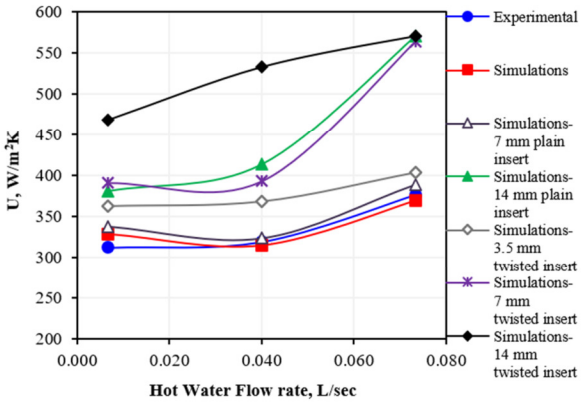

Fig. 7. *U* versus hot water flow rate.

C. Effect of Inserts on the Pressure Drop

Figure 8 presents the simulation predictions, which demonstrate a comparison of pressure drop for the cases in which different types of inserts were used and for the case in which no insert was present within the tube. In the absence of an insert within the tube, the pressure drop within the inner tube was observed to range from 12.21 Pa to 212.12 Pa across the three corresponding runs, designated as 1, 2, and 3, respectively. However, the introduction of inserts resulted in an increase in pressure drop. The pressure drop was relatively high for the cases in which 14 mm plain and twisted star-shaped inserts were used. The introduction of the twisted star-shaped insert resulted in a notable increase in pressure drop, reaching the highest recorded values of 149.44 Pa, 1157.73 Pa, and 2276.33 Pa for runs 1, 2, and 3, respectively. This was due to the fact that the inserts with a diameter of 14 mm occupied the greatest amount of space within the tube, thereby resulting in a significant pressure drop. As shown in Figures 7 and 8, the highest value of *U* was observed when a 14 mm twisted star-shaped insert was used. However, this resulted in the highest pressure drop. The lowest pressure drop was evidenced in the case of the 3.5 mm twisted star-shaped insert, although the *U* was also relatively low in that case. Moreover, the data presented in Figures 7 and 8 demonstrate that the usage of the 7 mm diameter twisted star-shaped insert resulted in a notable enhancement in the heat transfer rate and a relatively low pressure drop. At the maximum hot water flow rate of 0.073 L/s, when the 7 mm twisted inserts were used, the maximum

value of U was observed to be 564.40 W/m²K, while the pressure drop was 851.07 Pa. Similarly, for the hot water flow rate of 0.007 L/s, the U was 390.89 W/m²K, while the pressure drop was 35.30 Pa. In the absence of an insert, the U-value was 328.66 W/m²K and the pressure drop was 12.21 Pa. This demonstrates that the 7 mm twisted star-shaped insert can be employed to augment the heat transfer rate with a comparatively minimal increase in the pressure drop. These findings are crucial for optimizing the heat exchanger's design and ensuring efficient heat transfer.

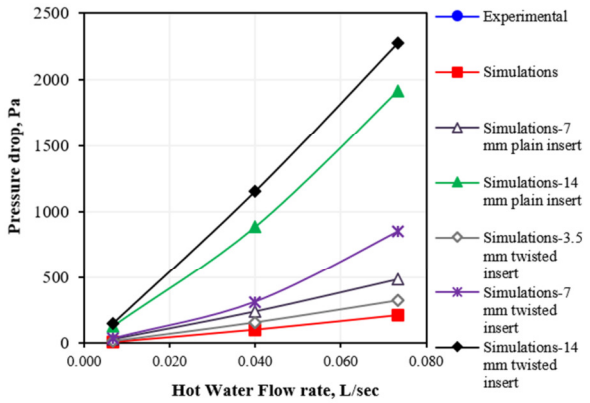

Fig. 8. U versus hot water flow rate.

D. Velocity Vector Analysis

Figure 9 presents the typical flow pattern inside the inner tube of the U-bend concentric heat exchanger, as predicted by CFD for run 1 condition when the hot water flow rate was 0.007 L/s (0.044 m/s). The velocity vector has illustrated the flow pattern, which offers insights into the fluid dynamics within the inner tube of the device. Figure 9(a) depicts the flow distribution within the tube in the absence of an insert. The fluid was distributed evenly throughout the tube, with a maximum velocity of 0.044 m/s observed in the central zone, which was consistent with the inlet conditions. The velocity of the fluid in the vicinity of the tube wall was relatively low due to the resistance exerted by the wall, with a range from 0.020 m/s to 0.030 m/s. Figure 9(b) shows the typical flow pattern inside the tube when a plain star-shaped insert with a diameter of 7 mm was employed. It was observed that the velocity profile underwent a transition into a higher secondary velocity along the length of the insert. The insertion of the aforementioned insert resulted in a reduction of the fluid flow area, as well as a change in direction at the edges due to the star-shaped configuration. These two factors generated a secondary fluid velocity, which induced turbulence and resulted in an enhanced heat transfer rate, attributed to a relatively high pressure drop. The maximum fluid velocity was noted to range between 0.050 m/s and 0.060 m/s, as evidenced by the presence of green and yellow velocity vectors. Similarly, Figure 9(c) portrays the fluid flow pattern inside the tube when a twisted star-shaped insert with a diameter of 7 mm was used. The fluid flow was primarily directed towards the sides and along the twisted edges of the insert. The secondary flow was generated as a result of the swirl motion and confined nature of the fluid's path. The swirl motion led to the generation of a secondary flow with a higher velocity, as observed from the velocity vectors, which were predominantly yellow and orange in color, indicating fluid velocities ranging from 0.060 m/s to 0.070 m/s. This resulted in the induction of high turbulence and a heightened heat transfer rate.

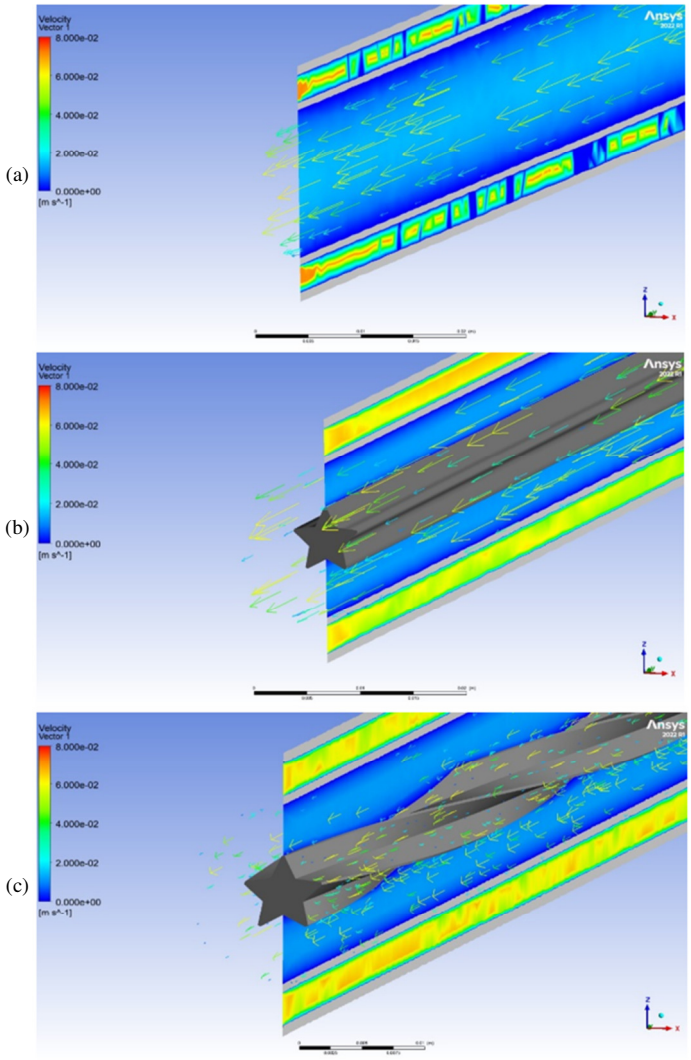

Fig. 9. Velocity vector analysis: (a) inner tube without insert, (b) inner tube with plain star shape insert, (c) inner tube with twisted star shape insert.

Figure 10 presents the intricate flow pattern and swirl motion of the fluid as it traverses the twisted star-shaped insert. The velocity vectors demonstrated in the figure are predominantly represented by yellow and orange hues as they pass through the edges of the insert. This was due to the fact that the direction of the flow was changing, and because of the confined nature of the area, turbulence was induced, resulting in the generation of a secondary flow with a relatively higher velocity.

IV. CONCLUSIONS

The effect of changing variables, specifically the inclusion of inserts, on the overall heat transfer coefficient (U) and the

pressure drop inside the inner tube of a U-bend concentric tube heat exchanger was examined through both experimental and computational means.

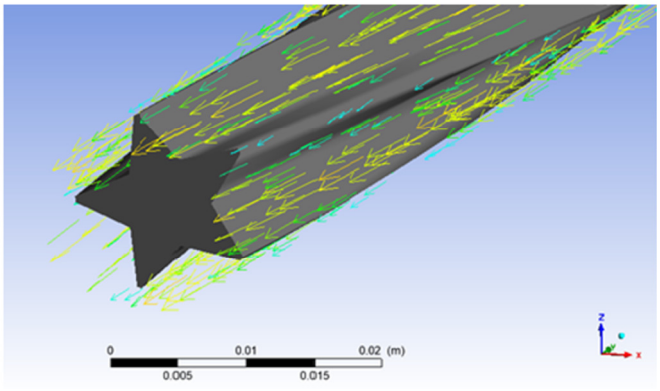

Fig. 10. Flow pattern along the twisted star shape insert.

Moreover, Computational Fluid Dynamics (CFD) simulations were employed to elucidate the internal dynamics of the system. The initial experiments were conducted in accordance with the design of experiment software. The device was modeled using CFD through ANSYS Fluent software, and simulations were performed for the corresponding experimental conditions. Following the successful validation of the experimental results and CFD predictions, a new set of CFD simulations was conducted to examine the impact of five distinct star-shaped inserts on *U* and pressure drop within the U-bend concentric tube heat exchanger. A systematic approach was employed to investigate, through simulations, the impact of a specific insert shape and size on both *U* enhancement and the simultaneous increase in pressure drop. The objective is to identify the optimal configuration, which should provide a higher *U* and a low pressure drop. Furthermore, the simulations provided insight into the internal dynamics of the system, demonstrating the secondary, higher fluid velocity induced by the inserts within the tube. The results demonstrate that the enhancement of the *U*-value is contingent upon the inclusion of inserts. The maximum *U*-values were observed to be 381.21 W/m²K and 468.96 W/m²K, respectively, with 14 mm plain and twisted star-shaped inserts at a hot water flow rate of 0.007 L/s. The inserts generated a secondary fluid motion inside the tube, which induced turbulence, and thus enhanced the heat transfer rate. In the case of the twisted tube star shape insert, the swirl motion induced higher turbulence, and hence a higher *U* was obtained. However, the turbulence induced inside the tube was attributed to a high pressure drop inside the tube. The highest pressure drop, 129.27 Pa and 149.44 Pa, was observed with the plain and twisted star-shaped inserts, respectively, at a hot water flow rate of 0.007 L/s. The twisted star shape insert of 7 mm was found to yield the optimal results, as evidenced by a *U*-value of 390.89 W/m²K and a pressure drop of 35.30 Pa at a flow rate of 0.007 L/s. Moreover, at a hot water flow rate of 0.073 L/s, the 7 mm twisted star shape insert yielded a *U*-value of 564.40 W/m²K, which was nearly equivalent to that of the 14 mm plain star shape insert, at a relatively low pressure drop of 851.07 Pa in comparison to 1918.34 Pa. Vector analysis demonstrated that the twisted star shape insert generated a flow pattern with a maximum velocity due to the swirl motion.

ACKNOWLEDGEMENT

The authors extend their appreciation to the Deanship of Scientific Research at Northern Border University, Arar, KSA for funding this research work through the project number "NBU-FFR-2024-1902-01." The authors acknowledge the Department of Chemical Engineering, University of Engineering and Technology, Peshawar Pakistan for providing the resources to carry out the experimental work.

REFERENCES

[1] B. Kumar, G. P. Srivastava, M. Kumar, and A. K. Patil, "A review of heat transfer and fluid flow mechanism in heat exchanger tube with inserts," *Chemical Engineering and Processing - Process Intensification*, vol. 123, pp. 126–137, Jan. 2018, https://doi.org/10.1016/j.cep.2017.11.007.

[2] P. Dradhomar, S. Verma, V. Singh, P. Dradhomar, and M. Manjunatha, "CFD analysis of double tube helical coil heat exchanger for different heat transfer characteristics," *International Journal of Advanced Research*, vol. 5, no. 4, pp. 1752–1757, Apr. 2017, https://doi.org/10.21474/IJAR01/4006.

[3] S. Naveen and S. Bhuvaneshwaran, "CFD Analysis of Concentric Tube Heat Exchanger Using Twisted Tapes," *International Journal of Advance Research, Ideas and Innovations in Technology*, vol. 3, no. 1, pp. 870–879, Feb. 2017.

[4] E. Edreis and A. Petrov, "Types of heat exchangers in industry, their advantages and disadvantages, and the study of their parameters," *IOP Conference Series: Materials Science and Engineering*, vol. 963, no. 1, Nov. 2020, Art. no. 012027, https://doi.org/10.1088/1757-899X/963/1/012027.

[5] M. M. Aslam Bhutta, N. Hayat, M. H. Bashir, A. R. Khan, K. N. Ahmad, and S. Khan, "CFD applications in various heat exchangers design: A review," *Applied Thermal Engineering*, vol. 32, pp. 1–12, Jan. 2012, https://doi.org/10.1016/j.applthermaleng.2011.09.001.

[6] B. Abdulmajeed and H. Jawad, "CFD Application on Shell and Double Concentric Tube Heat Exchanger," *Journal of Engineering*, vol. 25, no. 2, pp. 136–150, Jan. 2019, https://doi.org/10.31026/j.eng.2019.02.09.

[7] M. Guidi, P. H. Seeberger, and K. Gilmore, "How to approach flow chemistry," *Chemical Society Reviews*, vol. 49, no. 24, pp. 8910–8932, Dec. 2020, https://doi.org/10.1039/C9CS00832B.

[8] A. Nouri-Borujerdi and M. Layeghi, "A Review of Concentric Annular Heat Pipes," *Heat Transfer Engineering*, vol. 26, no. 6, pp. 45–58, Jul. 2005, https://doi.org/10.1080/01457630590950934.

[9] S. Quadri and S. S. J. Sheikh, "Evaluating the Performance of Concentric Tube Heat Exchanger With And Without Dimples By Using Cfd Analysis," *IOSR Journal of Mechanical and Civil Engineering*, vol. 13, no. 5, pp. 46–52, May 2016, https://doi.org/10.9790/1684-1305074652.

[10] K. Silaipillayarputhur, T. A. Mughanam, A. A. Mojil, and M. A. Dhmoush, "Analytical and Numerical Design Analysis of Concentric Tube Heat Exchangers – A Review," *IOP Conference Series: Materials Science and Engineering*, vol. 272, no. 1, Dec. 2017, Art. no. 012006, https://doi.org/10.1088/1757-899X/272/1/012006.

[11] V. Kumar, S. Saini, M. Sharma, and K. D. P. Nigam, "Pressure drop and heat transfer study in tube-in-tube helical heat exchanger," *Chemical Engineering Science*, vol. 61, no. 13, pp. 4403–4416, Jul. 2006, https://doi.org/10.1016/j.ces.2006.01.039.

[12] S. Liu and M. Sakr, "A comprehensive review on passive heat transfer enhancements in pipe exchangers," *Renewable and Sustainable Energy Reviews*, vol. 19, pp. 64–81, Mar. 2013, https://doi.org/10.1016/j.rser.2012.11.021.

[13] A. A. Kapse, V. C. Shewale, S. D. Barahate, A. B. Kakade, and S. J. Surywanshi, "Experimental Investigation of Heat Transfer and Pressure

Drop Performance of a Circular Tube with Coiled Wire Inserts," *Engineering, Technology & Applied Science Research*, vol. 14, no. 1, pp. 12512–12517, Feb. 2024, https://doi.org/10.48084/etasr.6551.

[14] M. Baig, I. Nouzil, A. Sheik, F. Mohammed, and Thameez, "Heat Transfer Augmentation in Concentric Tube Heat Exchanger Using Twisted Tapes," *International Journal of Engineering Research and Applications*, vol. 3, no. 3, pp. 1491–1496, May 2013.

[15] K. V. Warghat and H. D. Jagdale, "Heat transfer enhancement in concentric tube heat exchanger with tangential injection and twisted tape inserts," *Journal of Physics: Conference Series*, vol. 1473, no. 1, Feb. 2020, Art. no. 012032, https://doi.org/10.1088/1742-6596/1473/1/012032.

[16] M. Bahiraei, K. Gharagozloo, and H. Moayedi, "Experimental study on effect of employing twisted conical strip inserts on thermohydraulic performance considering geometrical parameters," *International Journal of Thermal Sciences*, vol. 149, Mar. 2020, Art. no. 106178, https://doi.org/10.1016/j.ijthermalsci.2019.106178.

[17] M. N. Abdullah, "Heat Transfer and Pressure Drop in Turbulent Flow through an Eccentric Converging-Diverging Tube with Twisted Tape Inserts," *Journal of Engineering and Sustainable Development*, vol. 16, no. 2, pp. 178–192, Jun. 2012.

[18] A. Yadav, "Effect of Half Length Twisted-Tape Turbulators on Heat Transfer and Pressure Drop Characteristics inside a Double Pipe U-Bend Heat Exchanger," *Jordan Journal of Mechanical and Industrial Engineering*, vol. 3, no. 1, pp. 17–22, Jan. 2009.

[19] A. S. Ambekar, R. Sivakumar, N. Anantharaman, and M. Vivekenandan, "CFD simulation study of shell and tube heat exchangers with different baffle segment configurations," *Applied Thermal Engineering*, vol. 108, pp. 999–1007, Sep. 2016, https://doi.org/10.1016/j.applthermaleng.2016.08.013.

[20] P. Naphon and T. Suchana, "Heat transfer enhancement and pressure drop of the horizontal concentric tube with twisted wires brush inserts," *International Communications in Heat and Mass Transfer*, vol. 38, no. 2, pp. 236–241, Feb. 2011, https://doi.org/10.1016/j.icheatmasstransfer.2010.11.018.

[21] K. K. Varma, P. S. Kishore, and T. Tirupathi, "CFD Analysis for the Enhancement of Heat Transfer in a Heat Exchanger with Cut Twisted Tape Inserts," *SSRG International Journal of Mechanical Engineering*, vol. 375, pp. 146–152, May 2017.

[22] A. G. Kanaris, A. A. Mouza, and S. V. Paras, "Flow and Heat Transfer Prediction in a Corrugated Plate Heat Exchanger using a CFD Code," *Chemical Engineering & Technology*, vol. 29, no. 8, pp. 923–930, 2006, https://doi.org/10.1002/ceat.200600093.

[23] R. Saini, B. Gupta, A. Prasad Shukla, B. Singh, P. Baredar, and A. Bisen, "CFD analysis of heat transfer enhancement in a concentric tube counter flow heat exchanger using nanofluids (SiO2/H2O, Al2O3/H2O, CNTs/H2O) and twisted tape turbulators," *Materials Today: Proceedings*, vol. 76, pp. 418–429, Jan. 2023, https://doi.org/10.1016/j.matpr.2022.12.044.

[24] R. Aridi, S. Ali, T. Lemenand, J. Faraj, and M. Khaled, "CFD analysis on the spatial effect of vortex generators in concentric tube heat exchangers – A comparative study," *International Journal of Thermofluids*, vol. 16, Nov. 2022, Art. no. 100247, https://doi.org/10.1016/j.ijft.2022.100247.

[25] S. Ali, J. Faraj, and M. Khaled, "A correlation for U-value for laminar and turbulent flows in concentric tube heat exchangers," *International Journal of Thermofluids*, vol. 23, Aug. 2024, Art. no. 100797, https://doi.org/10.1016/j.ijft.2024.100797.